ADVANCED FUNCTIONAL MATERIALS
www.afm-journal.de

Micrometer-Thin Nanocellulose Foils for 3D Organic Electronics

Marie Betker, Tim Erichlandwehr, Benedikt Sochor, Elisabeth Erbes, Alisher Kurmanbay, Yamit Alon, Yanan Li, Irene Fernandez-Cuesta, Peter Müller-Buschbaum, Simone A. Techert, L. Daniel Söderberg, and Stephan V. Roth**

Cellulose is a natural polymer with great properties such as high optical transparency and mechanical strength, flexibility, and biodegradability. Hence, cellulose-based foils are suitable for the replacement of synthetic polymers as substrate materials in organic electronics. This article reports the fabrication of ultrathin, free-standing cellulose foils by spraying aqueous 2,2,6,6-tetramethylpiperidine-1-oxyl-nanocellulose (TEMPO) fibrils ink layer-by-layer on a hot substrate using a movable spray nozzle. The resulting foils are only 2 ± 1 µm in thickness with an average basis weight of 1.9 g m^{-2}, which ranges in the same scale as the world's thinnest paper. The suitability of these ultra-thin nanocellulose foils as a sustainable substrate material for organic electronic applications is demonstrated by testing the foils resistance against organic solvents. Furthermore, silver nanowires (AgNWs) and the blend poly(3,4-ethylenedioxythiophene):polystyrene sulfonate (PEDOT:PSS) are integrated into the foils, and the foils are molded into 3D paper structures in order to create conductive, paper-based building blocks for organic electronics.

1. Introduction

Tengu joshi, a special kind of traditional paper prepared by Japanese handcrafters, is known as the world's thinnest paper. The origin of this paper dates back roughly a thousand years ago. It is made out of *"kōzo"*, bast fibers from the bark of mulberry trees. *Kōzo* are obtained via alkaline cooking. During this process water-soluble components, lignin, and hemi cellulose are removed, the bark becomes soft and is separated by beating with wood sticks into fibers, which mainly consist of cellulose. Subsequently, the fibers are rinsed, bleached, and made into paper. The resulting papers have a basis weight (≥2 g m^{-2}), translucent, and often porous with a fabric-like structure. Their main field of use is restoration and conservation of old documents, or by artists and designers as part of their art and installations.[1,2]

Fascinated by these old artistic paper-handcrafts, for the present study we investigated the implementation of TEMPO oxidized cellulose nanofibers (TCNFs) for the fabrication of continuous, free-standing, transparent cellulose foils in the same size range as *Tengu joshi* using a facile and more importantly scalable spray deposition technique. TCNFs have been chemically modified using a selective oxidation process mediated by TEMPO. This process introduces negative charges on the fibrils' surface, thus enhancing their stability and dispersibility in water.[3,4]

M. Betker, T. Erichlandwehr, B. Sochor, E. Erbes, S. A. Techert, S. V. Roth
Deutsches Elektronen Synchrotron DESY
Notkestraße 85, 22607 Hamburg, Germany
E-mail: stephan.roth@desy.de
M. Betker, A. Kurmanbay, Y. Alon, L. D. Söderberg, S. V. Roth
Fibre and Polymer Technology
KTH Royal Institute of Technology
Teknikringen 56–58, Stockholm 11428, Sweden
E-mail: dansod@kth.se

The ORCID identification number(s) for the author(s) of this article can be found under https://doi.org/10.1002/adfm.202403952

DOI: 10.1002/adfm.202403952

T. Erichlandwehr, I. Fernandez-Cuesta
Institute of Nanostructure and Solid State Physics (INF)
Hamburg Advanced Research Centre for Bioorganic Chemistry
Universität Hamburg
Luruper Chaussee 149, 22761 Hamburg, Germany
E. Erbes, S. A. Techert
Institute for X-ray Physics
Goettingen University
Friedrich Hund Platz 1, 37077 Goettingen, Germany
Y. Li, P. Müller-Buschbaum
Chair for Functional Materials
TUM School of Natural Sciences
Technical University of Munich
James-Franck-Straße 1, 85748 Garching, Germany
L. D. Söderberg
Wallenberg Wood Science Center
KTH Royal Institute of Technology
Teknikringen 52, Stockholm 10044, Sweden

This kind of cellulose has gained significant attention in material science due to its remarkable properties. Its biodegradability and bioavailability ensure minimal environmental impact. Additionally, cellulose-derived materials have shown exceptional resistance against mechanical stress, enabling the production of robust foils and fibers.[5,6] This unique combination of wood-based origin, biodegradability, transparency, and mechanical strength makes cellulose a promising material with a diverse range of applications such as sustainable packaging, actuators, medical applications, sensors, textiles, and organic electronics.[7–15]

For the fabrication of such flexible electronic devices ultrathin substrates are crucial, due to their higher transparency, lower weight, and small bending radius. Here, synthetic polymers are often used, because of their high optical transparency, great mechanical properties, and resistance against chemicals. Common examples are poly(ethylene terephthalate) (PET), polyimide (PI), Polydimethylsiloxane (PDMS), or polymethyl methacrylate (PMMA) foils. These foils are commercially available in a broad range of thicknesses from 1.4 µm up to several hundreds of micrometers.[16] For example, Kim et al. used two spin coated 1.5 µm thin PI films to encapsulate a thin-film transistors from both sides, achieving a bending radius of only 0.25 mm.[17] Unlike PET and PMMA, PI is a colored polymer and therefore not the most favorable choice for transparent electronics. Kumaresan et al. reported a 1.9 µm thin film of spin coated PMMA as substrate for gas sensors.[18] However, PMMA is soluble in organic solvents, which can be beneficial for usage as a sacrificial layer,[19] but needs special consideration when used as substrate material in fabrication processes which utilize organic solvents. PET is one of the most used polymers in this field due to its numerous properties appropriate for flexible, transparent electronics. It is highly transparent, has no color, is mechanical stable, and cannot be dissolved easily, to name a few. For example, Garnier et al. printed a field-effect transistor on top of a 1.5 µm PET substrate.[20] Although there are ways to recycle PET industrially, it is not a biodegradable plastic under normal environmental conditions like natural polymers.[21] Natural occurring polymers like cellulose and silk are more eco-friendly than synthetic polymers due to their biodegradability and meet the same requirements for fabrication of flexible electronics: Fukuzumi et al. prepared 20 µm thin films via suction filtration of TEMPO-cellulose fibers from softwood. The films were highly transparent (90% at 600 nm) and showed exceptional mechanical properties with a Young's modulus of 6.9 ± 1.4 GPa and tensile strength of 233 ± 44 MPa.[22] Lei et al. fabricated ultrathin (800 nm) cellulose substrates for flexible, disintegrable transistors and circuits. First, they modified microcrystalline cellulose powder to get trimethylsilyl-functionalized cellulose in chlorobenzene, which was spin coated onto a sacrificial layer. Second, the resulting film was treated with acid vapor to get a hydrolyzed cellulose film, which was finally put into water to dissolve the sacrificial layer. The substrate showed an outstanding transmission of up to 98% in the range of 400 to 1800 nm and a surface roughness of 3.9 nm.[23] However, in order to compete with ultrathin synthetic polymer films, the fabrication process must be as fast and facile as possible. The excessive usage of dangerous chemicals should be avoided, and the operation of complicated techniques and costly machines should be minimized. There are several strategies to fabricate cellulose-based free-standing foils. The two main techniques are casting and filtration, often in combination with heating, applied pressure, under vacuum, or with freeze drying in order to remove the water faster. The fabrication method dictates the final morphology and properties of the foils. To facilitate the fabrication of ultrathin TCNF foils for electronic applications we used spray-deposition. This method involves the atomization and deposition of a liquid onto a target, enabling the uniform coating of substrates or the fabrication of thin-films over large areas. Its scalability makes it suitable for production on an industrial scale, offering efficient and time-saving deposition of materials, high throughput, and therefore cost-effectiveness.[24–26] Therefore, spray deposition has also emerged as a scalable, rapid, and facile technique for various applications in material sciences. For example, Shanmugam et al. reported the fast and effort-saving fabrication of nanocellulose films using spray deposition.[27] They achieved papers of different basis weights between 38 g m^{-2} up to 187 g m^{-2} by simply adjusting the consistency of the cellulose suspension and operating speed.[25] Beneventi et al. sprayed cellulose films (124 g m^{-2}) with a strain at break of 150 MPa and a Young's modulus of 18 GPa. They found, that these great mechanical properties decrease with decreasing basis weight.[26]

Here, we report the fabrication of three-dimensional (3D), curved paper structures made of ultrathin TCNF foils. In the context of cellulose processing for foils, we used a novel fabrication method, which includes spraying an aqueous TCNF dispersion using a horizontally moving spray nozzle layer-by-layer onto a silicon wafer as substrate. Subsequently, the dry TCNF films were delaminated without the need of a sacrificial layer in a water bath to obtain self-supporting, ultrathin TCNF foils. No dangerous chemicals nor complicated additional techniques were used in the process. We demonstrate the suitability of these foils as sustainable substrate material by molding them into conductive, 3D paper structures. In addition to that, we tested the resistance of the foils against chemical solvents. Our results prove the general applicability of our approach to fabricate freestanding, ultrathin, bio-based functional materials.

2. Results and Discussion

The sprayed TCNF foils (**Figure 1a**) are transparent (80–90%) in the wavelength range of 400 nm $\leq \lambda \leq$ 1000 nm, which is in the same range as other recently published TCNF thin films,[28–30] and show thin-film interference effects depending on their local thickness (Figure 1b). Due to their average thickness of only 2 ± 1 µm (Figure S2, Supporting Information), these foils demonstrate an average basis weight of only 1.9 ± 0.9 g m^{-2}, which is to the best of our knowledge the lowest reported value for cellulose foils, as compared in **Table 1**. SEM imaging (Figure 1c) reveals the arrangement of TCNF as long fibers in a non-ordered manner with ≈ 2.5% of the surface area filled with circular-like pores of 56 ± 2 nm^2 average area (Figure S3, Supporting Information), which corresponds to an average diameter of 8.4 nm. Results from AFM measurements (Figure 1d) reveal a very low RMS roughness of only 5 ± 1 nm. It is interesting to note that these results are in the same range as in our previous published work where the sprayed TCNF films were roughly ten times thinner than in this work.[31] Grazing incidence wide angle X-ray scattering (GIWAXS) data (Figure 1e; Figure S4, Supporting Information)

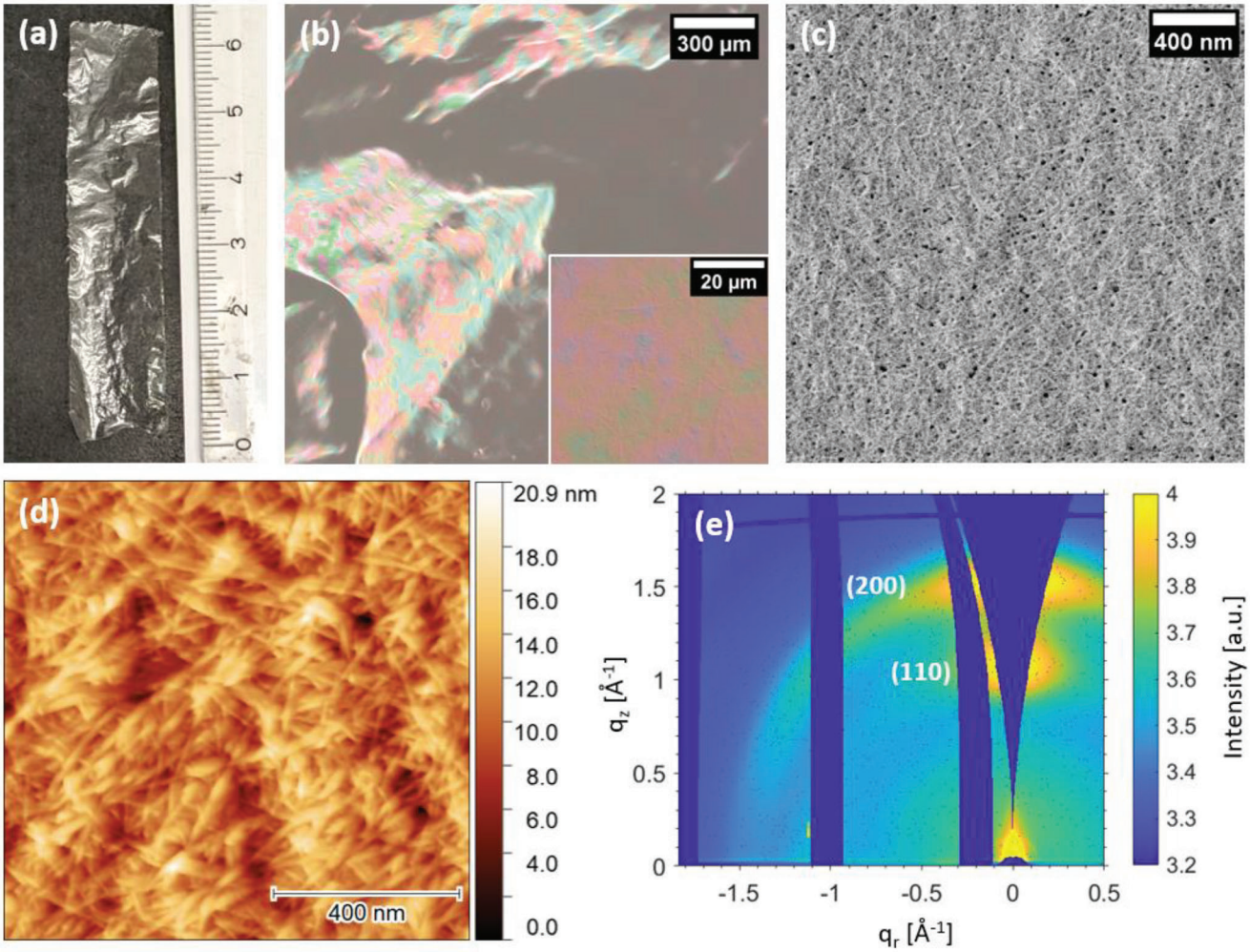

Figure 1. Multiscale structural analysis of sprayed TCNF foil from macroscopic scale down to molecular scale. Photograph of TCNF foil a) demonstrates the possibility of large-scale fabrication of sprayed TCNF foils. Optical microscopy images b) show its thin-film interference. SEM image c) and AFM image d) show the nanostructured surface of TCNF foils and the arrangement of TCNF in long nanofibers. 2D GIWAXS data e) shows the two crystallographic orientations (200) and (110) in TCNF.

shows the two well-known[32] crystal planes (200) and (110) of cellulose at 1.09 Å^{-1} and 1.53 Å^{-1}, respectively.

2.1. Functional TCNF Foils

To demonstrate the suitability of the paper fabricated in the present study as sustainable substrate foils for organic electronics, we added AgNWs and the polymer blend PEDOT:PSS as functional building blocks to our TCNF foils (Figure S1 in the Supporting Information). We term these foils "functional TCNF foils". We used our previously published[31] cellulose-based AgNW-CNF ink to fabricate conductive TCNF foils (**Figure 2**). Here, we tested three different foil compositions, namely coated, multilayer, and mixed TCNF-based foils: Transparent AgNW-TCNF foils were fabricated by spraying AgNW-CNF ink on top of the TCNF foils. These foils are termed "Top AgNW-TCNF". Non-transparent AgNW-TCNF foils were fabricated by spraying TCNF and AgNW-CNF ink layer-by-layer alternately. These foils are termed "Embedded AgNW-TCNF". Besides silver, we incorporated also PEDOT:PSS by spraying a mixed ink of TCNF and PEDOT:PSS in water, which are termed "PEDOT:PSS-TCNF".

Top AgNW-TCNF have a shiny, translucent, silvery finish (Figure 2a). The AgNWs are well dispersed on the surface of the foil (Figure 2d). These foils are transparent (> 60%), but they are also more prone to folding/twisting in terms of electric resistance (Video S1, Supporting Information), which indicates

Table 1. Comparison of basis weight and thickness of TCNF foils obtained here with previous published sprayed cellulose foils.

Reference	Thickness [µm]	Basis weight [g m^{-2}]
This work	2.0 ± 1	1.9 ± 0.9
D. Beneventi et al. (2014)[33]	6.5 ± 1	8.0
D. Beneventi et al. (2015)[26]	~10.0	13.7
K. Shanmugam et al. (2018)[25]	58.4	38.0
H. Nadeem et al. (2020)[34]	64-74	37.0 ± 0.9
K. Shanmugam et al. (2017)[27]	83.9 ± 13.9	52.8 ± 7.4

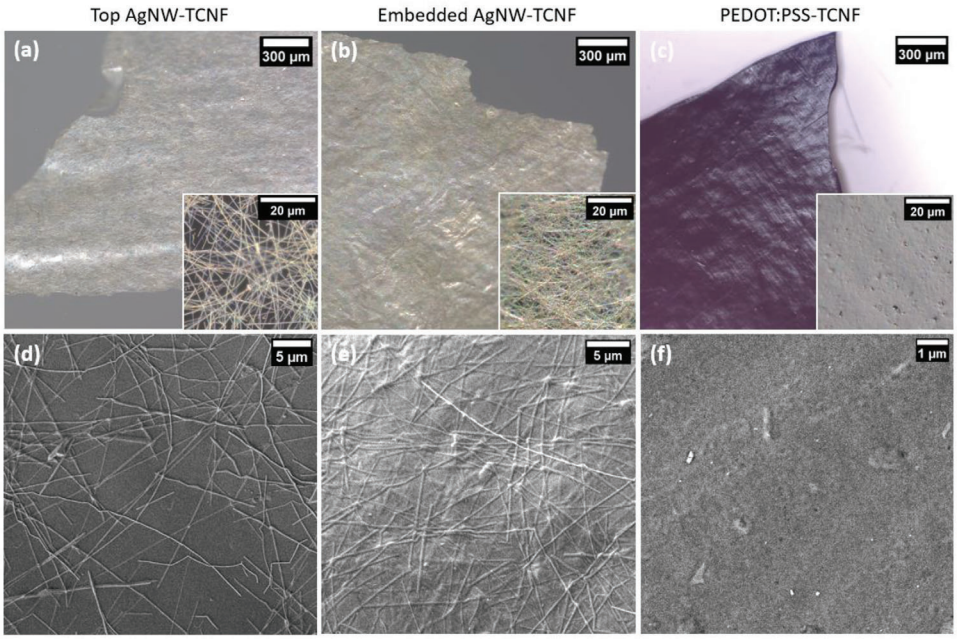

Figure 2. Structural analysis of functional TCNF foils with AgNWs sprayed on top (a+d), with integrated AgNWs (b+e), and with integrated PEDOT:PSS (c+f). Optical microscopy images a–c) show the overall morphology of the TCNF-based foils, the insets show the microstructure, and SEM images d–f) show the nanostructured surfaces of all three foils.

reversible rearrangements of the conductive AgNW network. Embedded AgNW-TCNF show a shiny, metallic finish (Figure 2b). The AgNWs form a very densely packed network, which makes these foils almost non-transparent (< 20%). However, these foils are more robust due to the embedded AgNWs inside the TCNF foil and demonstrate very stable values of resistance (<10 Ω cm^{-1}) under folding/twisting (Video S2, Supporting Information). It is interesting to note, that the delamination in water did not affect the electric conductivity of the AgNW-based foils. Naturally, the values of transparency and resistance of both types of AgNW-TCNF foils depend on the number of sprayed layers (**Figure 3a**) and can easily be adjusted to the desired values using spray deposition. We discussed the correlation between AgNW content, sheet resistance, and transmittance of sprayed AgNW-TCNF electrodes in a previous publication in detail.[31]

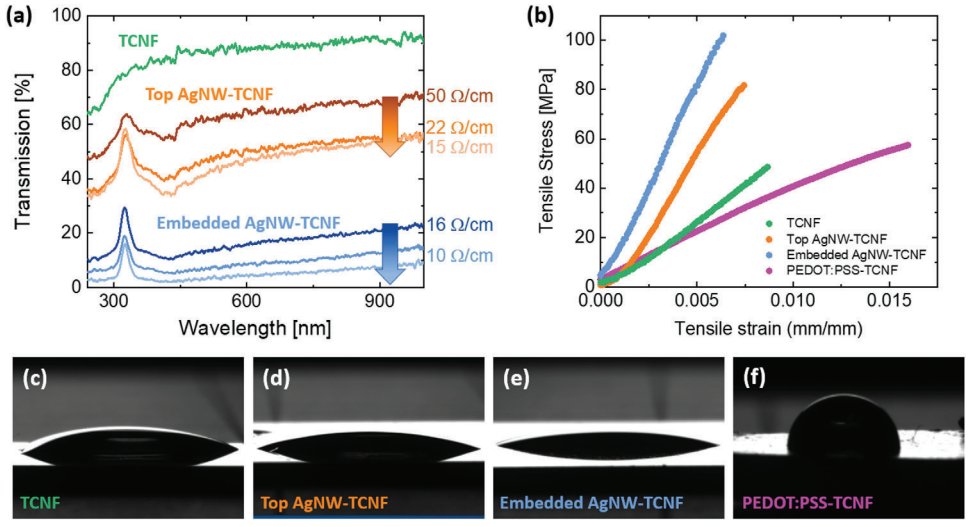

Figure 3. Properties of TCNF foils. UV–vis spectra a) of TCNF foil (green), Top AgNW-TCNF foils (orange color gradient) and Embedded AgNW-TCNF foils (blue color gradient). The arrows demonstrate the increasing concentration of AgNWs in the foils, hence their resistance and transmission are decreasing. The PEDOT:PSS-TCNF foil is not shown here because it is not transparent. Tensile testing yields stress-strain curves of the different foil types with average Young's modulus b). Water contact angle measurements for TCNF c), Top AgNW-CNF d), Embedded AgNW-TCNF e), and PEDOT:PSS-TCNF foils f).

Table 2. Properties of TCNF foils, AgNW-TCNF foils, and PEDOT:PSS-TCNF foils.

Foil type	Young's modulus [GPa]	Strain at break [mm mm^{-1}]	Tensile breaking strength [MPa]	Contact angle [°]	RMS roughness [nm(sq)]	Electric Conductivity [S m^{-1}]
TCNF	3.8 ± 1.1	0.009 ± 0.004	49 ± 1	34 ± 2°	5 ± 1	Not conductive
Top AgNW-TCNF	9.6 ± 1.0	0.007 ± 0.001	82 ± 14	28 ± 1°	25 ± 2	$4.2 \times 10^4 \pm 243$
Embedded AgNW-TCNF	10.9 ± 1.2	0.006 ± 0.001	102 ± 7	26 ± 3°	56 ± 2	$1.3 \times 10^5 \pm 195$
PEDOT:PSS-TCNF	4.0 ± 0.05	0.018 ± 0.004	57 ± 5	80 ± 3°	4 ± 1	22.3 ± 0.2

PEDOT:PSS-TCNF are not transparent and show a dark-blue color (Figure 2c). Their surface is very homogenous and uniform (Figure 2f). Polarized microscopy (Figure S5, Supporting Information) shows that there are no larger agglomerations and also no alignment of TCNF (Figure S5a, Supporting Information), PEDOT, or PSS (Figure S5h, Supporting Information) in the foils along a specific direction. This agrees with SEM and AFM measurements. However, while AgNWs in TCNF foils seem to be randomly distributed (Figure S5b,c, Supporting Information), polarized microscopy reveals that a certain amount of AgNWs are actually aligned in a network-like structure (Figure S5f,g, Supporting Information). In terms of electrical conductivity, Embedded AgNW-TCNF demonstrates the highest value ($1.3 \times 10^5 \pm 2.0 \times 10^2$ S m^{-1}, **Table 2**), followed by Top AgNW-TCNF ($4.2 \times 10^4 \pm 2.4 \times 10^2$ S m^{-1}), and PEDOT:PSS-TCNF (22 ± 0.2 S m^{-1}). Pure TCNF foils are not conductive. These findings prove the Embedded AgNW-TCNF and Top AgNW-TCNF foils as highly conductive, suitable for applications such as electromagnetic shielding[35,36] or in electrical circuits,[37] or supercapacitors.[38] PEDOT:PSS-TCNF foils need an additional treatment with organic solvents to increase their electrical conductivity, as shown later on in this report.

The mechanical properties (Figure 3b) of the different foil types are crucial for their use in flexible electronics. Pure TCNF foils show a Young's modulus of 3.8 ± 1.1 GPa and a strain at break at 0.0092 ± 0.0043 mm mm^{-1} (Table 2) at an average density of 0.95 g cm^{-3}. This result is on the lower end of comparable pure TCNF films such as of Wakabayashi et al. (1.6 GPa at a density of 0.56 g cm^{-3}),[39] and Beneventi et al. (16 GPa at 1.3 g cm^{-3})[33] due to the low density of TCNF foils. The addition of AgNWs and PEDOT:PSS into TCNF foils affected these properties. The addition of AgNWs increased Young's modulus (Top AgNW-TCNF = 9.6 ± 1.0 GPa; Embedded AgNW-TCNF = 10.9 ± 1.2 GPa), but at the same time decreased strain at break (Top AgNW-TCNF = 0.0067 ± 0.0014 mm mm^{-1}; Embedded AgNW-TCNF = 0.0064 ± 0.0008 mm mm^{-1}). This trend is also reflected in the tensile strength at break, which was roughly twice as high (82 ± 14 MPa for Top AgNW-TCNF, and 102 ± 7 MPa for Embedded AgNW TCNF) after addition of AgNWs into the foils. Adding PEDOT:PSS did not affect much the Young's modulus (4.00 ± 0.05 GPa) of TCNF foils, but increased its tensile strength from initially 49 ± 1 MPa to 57 ± 5 MPa, and made them more elastic, which increased the strain at break significantly (0.018 ± 0.004 mm mm^{-1}). This is an interesting result, because the strain of TCNF-PEDOT:PSS composites usually decreases with increasing PEDOT:PSS content.[40] The water contact angle (WCA) of TCNF foil was 34°, which is in accordance with previously published results of TCNF films.[4,41] Low WCA are typical for TCNF due to the high content of carboxy groups on their surface. With increasing AgNW content WCA decreased to 26° for Embedded AgNW-TCNF due to their rougher surface. PEDOT:PSS-TCNF foils showed the highest water contact angle of 88°. This finding is in accordance with previous findings of our group[42] where we tested the WCA of similar, not free-standing films of TCNF and PEDOT:PSS.

The topographies of the different functional foils are shown in **Figure 4**. AFM images of Top AgNW-TCNF and Embedded AgNW-TCNF look very similar (Figure 4a,b). The coverage of AgNWs with TCNF fibers can be clearly seen as the fuzzy nanostructures around the AgNW (Figure 4d,e). However, the two foils differ in surface roughness, because of their different bulk structure. For Top AgNW-TCNF, the AgNWs are only located on the surface and thus lead to an RMS roughness of 25 ± 2 nm. The AgNWs in Embedded AgNW-TCNF are distributed throughout the whole foil, which makes these foils twice as rough (56 ± 2 nm). In contrast to that, the presence of PEDOT:PSS in TCNF foils (Figure 4c,f) lowers the foils' roughness (4 ± 1 nm), since PEDOT:PSS nanoparticles fill in the porous TCNF matrix.

The fabrication of devices for organic electronics necessitates the use of different solvents. Some examples are dimethylsulfoxid C_2H_6OS (DMSO), isopropanol C_3H_8O (IPA), and methanol CH_3OH (MeOH),[43–45] to name just a few. Therefore, the chemical interactions of TCNF foils with organic solvents and their potential induced physical changes are very important. We tested the interaction of all foil types with these three different organic solvents, which range from non-toxic (DMSO, IPA) to toxic (MeOH). In general, any solvent will mostly interact with the accessible TCNF on the foils surface, but can also enter the bulk structure through pores in the foils' surface. The total solvent uptake is composed of the free solvent in the pores and the solvent molecules bond to the fibers. TCNF will sorb the solvent molecules by forming hydrogen bonds due to its hydroxy- and carboxyl groups present on the fibers' surface. The driving force of this process is a decrease of enthalpy, because during the sorption of solvent molecules energy is set free. The polarity of the solvents is crucial for their interaction with TCNF foils and is represented by their dielectric constant. The more polar, meaning the higher the dielectric constant of a solvent, the more hydrogen bonds can be formed and the stronger are the interactions between solvent and TCNF.[46,47] Here, DMSO is the most polar solvent with a dielectric constant of 47.0, followed by MeOH (32.6), and IPA (18.3).[45] However, MeOH and IPA are protic solvents, which means that these solvents can contribute to hydrogen bonding with cellulose by donating H^+ ions. But DMSO is an aprotic solvent, which means that it will not contribute as H^+ ions donor for hydrogen bonding. Hence, DMSO molecules do not from hydrogen bonds with cellulose or with themselves, but self-associate via dipole-dipole interactions of their highly polar

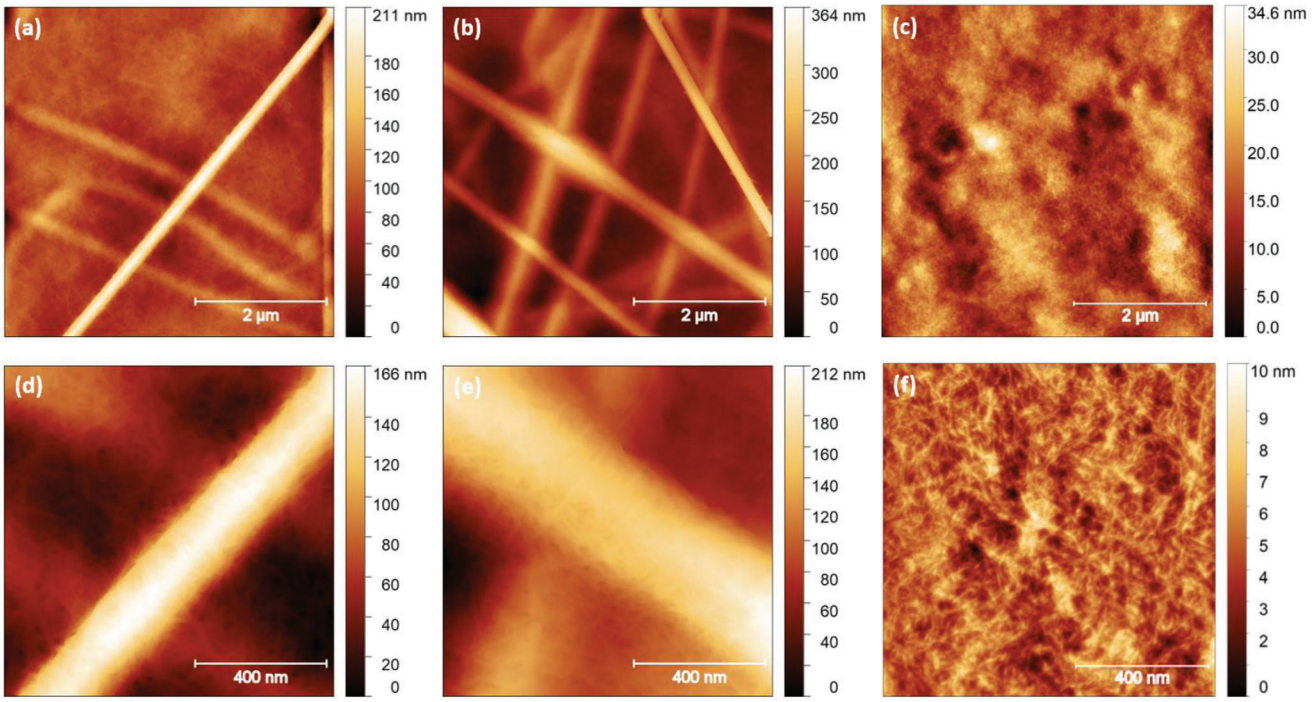

Figure 4. Atomic force microscopy images of functional TCNF foils: Top AgNW-CNF a,d), Embedded AgNW-TCNF b,e), and PEDOT:PSS-TCNF foils c,f).

sulfoxide groups. Because of this high polarity, DMSO molecules can form hydrogen bonds with water molecules, and here water acts as the H^+ ions donor. Therefore, DMSO molecules sorb to and mix with the water molecules present in the cellulose foils.

For the experiments, each tested TCNF foil was immersed in one of the solvents for two weeks, taken out, dried, and pressed for 24 hours. While in the solvent baths, TCNF foils kept their integrity and could be moved around without problem. The solvent-soaked foils could be taken out of the solvent baths without showing any damage or structural changes like wrinkles. In fact, foils which got folded or stuck together during take out could simply be rearranged or detached, as long as the foils were still soaked with solvent. In general, the handling of foils in MeOH was most challenging, since MeOH almost immediately evaporates. While taking the foils out of MeOH, only a few seconds remain to arrange the still soaked foils carefully in a spread-out manner. In addition, protection gear is necessary when working with methanol. This is not the case for DMSO, since it is a non-toxic solvent and has a high boiling point. Yet, the high boiling point is also a major drawback of DMSO: It does not evaporate under normal conditions, so that leftovers of DMSO will still be left in the TCNF foils. This can be bypassed by heating up the foils to the boiling point of DMSO (189 °C); however, cellulose also starts to degrade (weight loss) close to this temperature region.[48] The easiest-to-handle-foils are those immersed in IPA.

The Fourier-transform infrared spectroscopy (FTIR) analysis (**Figure 5a**) shows the characteristic peaks (-CH/-CH_2 at 2900 cm^{-1}, -COO^- at 1606 cm^{-1}, and the cellulosic backbone region from 1020–1160 cm^{-1}) of TEMPO cellulose for TCNF foil immersed in IPA, MeOH, DMSO, and water as a control group. The chemical structure of the foils did not change when immersed in the solvents. This finding can be explained as follows: Moisture is always present in air. Thus, water is already adsorbed to the cellulose hydroxyl groups (broad peak at 3298 cm^{-1}) of TCNF foils before immersion in organic solvents. Since water has the highest dielectric constant of all tested solvents, no solvent exchange takes place and water is still adsorbed to TCNF after immersion in organic solvents.[48,49]

The optical transmission in the wavelength range of 400 nm $\leq \lambda \leq$ 1000 nm of TCNF foils immersed in IPA, MeOH, and DMSO did not change significantly (Table S1, Supporting Information). Optical microscopy (Figure S6, Supporting Information) shows no change in the foils' composition. AFM measurements (Figure S7, Table S2, Supporting Information) show, that the roughness of the TCNF foils did not change significantly. GIWAXS studies (Figure S8, Table S3, Supporting Information) reveal, that the position of the crystalline planes (200) and (110) of TCNF foils did not change when IPA, MeOH, and DMSO were sprayed on top. Similar to water, the organic solvent molecules are too large to enter the crystalline parts of TCNF (1.09 $Å^{-1}$ and 1.53 $Å^{-1}$) and thus no change in arrangement of crystalline structure is observed. However, an increase in intensity was found for both peaks of IPA and MeOH, and for the (200) peak of DMSO, respectively), which indicates a slight increase in crystallinity. The (110) peak of DMSO treated foils neither changed in q position nor in intensity, but its FWHM increased significantly. We conclude that some DMSO was still left in the surface of TCNF foils during the measurements due to its high boiling point, leading to the broadening of the (110) peak.

The contact angle allows to estimate the potential for imbibition of droplets during spray deposition into TCNF foils. Hence, we analyzed the contact angle of the three different solvents. For

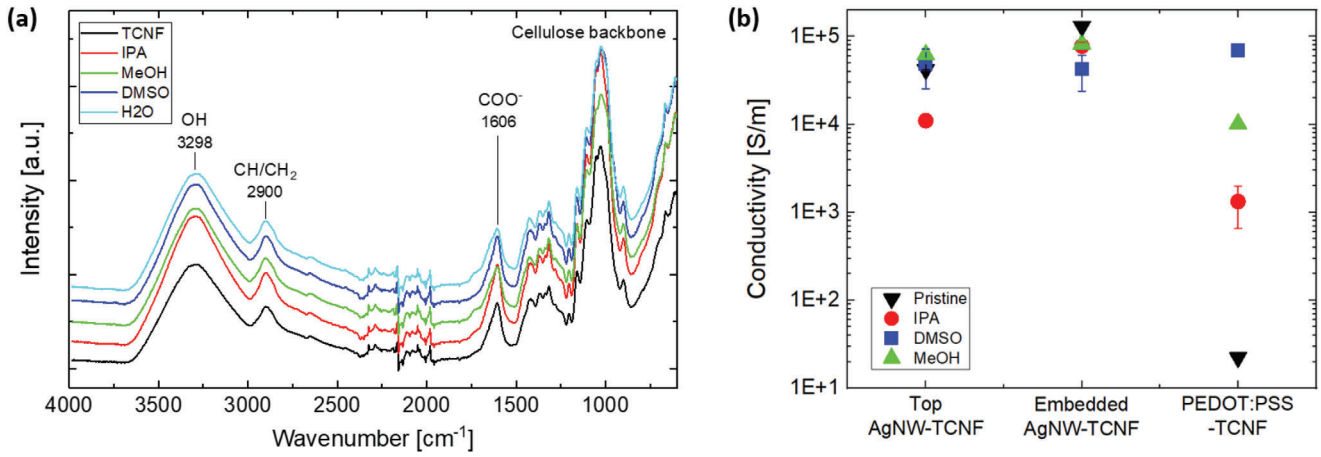

Figure 5. FTIR spectra of TCNF foil before (black line) and after immersion in organic solvents and water a). Conductivity plots of the functional foils before (pristine) and after immersion in organic solvents b). The spectra in (a) are shifted for clarity.

IPA and MeOH, no contact angle could be measured, since these solvents immediately wetted the foils surface and evaporated fast. Only DMSO showed a contact angle of 37 ± 1 ° for TCNF foils, 29 ± 1 ° for Top AgNW-CNF, 28 ± 1 ° for Embedded AgNW-TCNF, and 31 ± 2 ° for PEDOT:PSS-TCNF. Therefore, all contact angles of DMSO were roughly in the same range. This means, that the foils have a high wettability for the investigated solvents, favoring a more homogenous distribution of these solvents on the surface of TCNF foils.

Conductivity measurements show the influence of organic solvents on the electric conductivity of functional TCNF foils (Figure 5b, Table S4, Supporting Information). Here, the most prominent effect was observed for PEDOT:PSS-TCNF foils. Their conductivity increased several orders of magnitude from initially 22.3 ± 0.2 S m^{-1} to 7.0 × 10^4 ± 0.3 × 10^4 S m^{-1} after immersion in DMSO, and 1.0 × 10^4 ± 0.1 × 10^4 S m^{-1} in MeOH. This effect stems from the phase separation of PEDOT and PSS induced by polar organic solvents, leading to better connected PEDOT domains, which finally enhances the charge mobility and thus the conductivity of PEDOT:PSS-TCNF foils.[40,50] The least polar solvent IPA had also the least impact on the conductivity (1.3 × 10^3 ± 0.7 × 10^3 S m^{-1}) of PEDOT:PSS-TCNF foils. The initially high conductivity of embedded AgNW-TCNF foils (1.3 × 10^5 ± 195 S m^{-1}) decreased slightly in all three solvents, with DMSO showing the highest decrease (MeOH 8.2 × 10^4 ± 0.8 × 10^4 S m^{-1}, IPA 7.8 × 10^4 ± 0.8 × 10^4 S m^{-1}, DMSO 4.3 × 10^4 ± 1.9 × 10^4 S m^{-1}). For Top AgNW-TCNF foils (4.2 × 10^4 ± 2.4 × 10^2 S m^{-1}) immersion in IPA decreased the conductivity (1.1 × 10^4 ± 0.1 × 10^4 S m^{-1}) the most. IPA is a standard solvent for AgNWs. During immersion of AgNW-based foils in IPA, AgNWs presumably diffused back into the solvent again, so the conductive AgNW network in the foil was damaged, leading to a decrease in conductivity. For Top AgNW-TCNF this effect is much larger, since it has less AgNWs, and all AgNWs are located only on the foils' surface. The reason for the change in conductivity for MeOH and DMSO are unclear, but likely related to structural changes in the foils over time. For MeOH it can be the increase in roughness (see Table S2, Supporting Information), while for DMSO we suspect that there are still leftovers of this solvent left in the foil.

Finally, we tested the possibility of manufacturing 3D, macroscopic structures by forming 3D shapes out of the TCNF-based foils. Here, we made use of the hygroscopicity of TCNF, which is usually considered as a problem, since TCNF lose their great mechanical properties when in contact with water. However, we used this decrease in integrity of TCNF foils while immersed in water to arrange them into 3D shapes. To do so, we brought the freestanding foils into the desired 3D form while they were still wet and afterwards dried them overnight. With this simple technique, we were able to make curved, self-supporting 3D objects like waves, spirals, and stairs (**Figure** 6a,b,c) out of the different TCNF-based foils.

Due to their optical transparency, high conductivity, flexibility, and resistance to organic solvents, our foils can potentially be used in many fields. Here, we tested the Embedded AgNW-TCNF foil as an electrical conductor in a capacitor (Figure 6d). The capacitor was made by simply wrapping two of the Embedded AgNW-TCNF foils around each other, separated by a piece of Cellophan as a dielectric medium. It reached a capacitance of 30 ± 5 nF. We further investigated possible fields of application by measuring the change in electrical resistance of Top AgNW-TCNF and Embedded AgNW-TCNF (Figure 6e) foils under water exposure. To do so, we clamped the foils between two contacts of a multimeter and wetted the foil in the space between the two contacts by depositing 100 µL of water drop by drop. While Top AgNW-TCNF showed only a minor increase in line resistance over time (3.3 Ω cm^{-1} over 4.5 min, Figure S9a, Supporting Information), the Embedded AgNW-TCNF foils showed first a minimal decrease in resistance, followed by a return to the initial value (Figure S9b, Supporting Information). Top AgNW-TCNF foils contain more CNF. Since it is the CNF, which adsorbs the water, these foils are more prone to structural changes inside the foil due to moisture. A change in structure affects the conductive AgNW network in the foils and the conductivity decreases. Embedded AgNW-TCNF foils have less TCNF content and the AgNW network is more densely packed, which makes these foils more resistant to moisture.

The presented results show that our ultrathin, sprayed TCNF foils are versatile, lightweight materials, which can be coated with

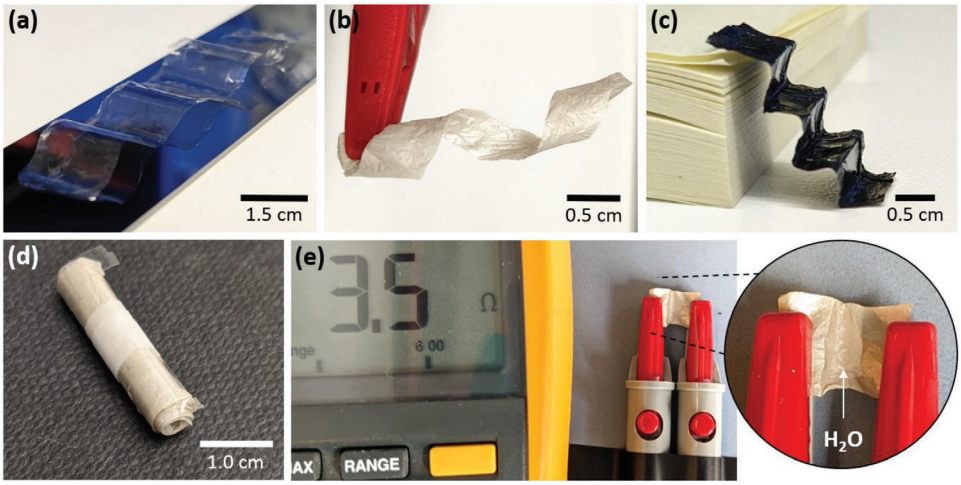

Figure 6. 3D structures formed out of TCNF foil a), Embedded AgNW-TCNF foil b), and PEDOT:PSS-TCNF foil c). A capacitor made of two Embedded AgNW-TCNF foils d). Electrical resistance of Embedded AgNW-TCNF foil while exposed to water e).

materials dissolved in organic solvents with only minor effects on the foils' structural and optical properties. Their chemical structure was not affected, and also the crystallinity and roughness did not change significantly. The possibility of integrating functional materials into, and forming 3D shapes out of these foils leads the way towards exciting possibilities in the field of sustainable, free-standing organic electronics.

3. Conclusion

We demonstrate the fabrication of the, to the best of our knowledge, thinnest (2 ± 1 µm) to date reported freestanding TCNF foils via layer-by-layer spray deposition of TEMPO-cellulose nanofibrils. The foils are highly transparent, very smooth, and, with a basis weight of only 1.9 g m^{-2}, ranging in the same scale as the world's thinnest paper. The delamination of TCNF foils takes place in water, and no special treatment or sacrificial layer is needed. The foils are true freestanding films without any support or frame needed. We show the applicability of these foils by forming curved, self-supporting 3D shapes out of them. Integrating functional building blocks like nanoparticles and polymers into the foils opens the possibility for a craft box full of lightweight, functional components of individual shapes and properties, which can be combined into paper-based, 3D electronic gadgets.

4. Experimental Section

Materials: Bleached, never dried sulfite pulp (Norway Spruce, Domsjö) was treated using 2,2,6,6-tetramethylpiperidine-1-oxyl (TEMPO) mediated oxidation according to the procedure published by Isogai et al.[4] The TEMPO-CNF gel was dispersed in ultrapure water (0.03 wt%) via mechanical mixing and sonification for 10 minutes. The resulting dispersion was centrifuged for 60 min at 5000 rpm. The final TCNFs had a diameter of around 4 nm, a length of around 500 nm, and the carboxylate content was 800 µmol g^{-1}. Silver nanowires (0.5 wt% in IPA; diameter = 100 nm, length up to 50 µm) and PEDOT:PSS (1.1% in H_2O) were purchased from Sigma Aldrich. To prepare the AgNW-TCNF ink the purchased silver nanowire dispersion was mixed with the previously prepared TCNF dispersion in a volume ratio of 1 to 10 by sonification for 2 minutes. To prepare the PEDOT:PSS-TCNF ink the purchased PEDOT:PSS dispersion was mixed with the previously prepared TCNF dispersion in a volume ratio of 1 to 1 by mechanical mixing overnight.

Substrate Preparation: Silicon wafers (one-side polished, boron doped (100), Si-Mat, Germany) were first washed with acetone, isopropanol, and ultrapure water (18.2 MΩ cm^{-1}), and then treated with UV-light and ozone (UV Ozone Cleaner, Ossila Ltd., UK) for 10 min. After cleaning, a frame consisting of PDMS was placed on the silicon wafer. The size of the frames determined the size of the final foils.

Sample Preparation: All foils were prepared via layer-by-layer spray deposition on heated (110 °C, EMS 1000 series, Electronic Microsystems) silicon wafers using a moving spray nozzle (Compact JAU D555000, Spray Systems Inc.) in combination with a motorized linear stage (LTS300/M, Thorlabs Inc.). The length of a single deposited layer corresponds to the full length of the sprayed foil, while the length of a double layer corresponds to twice the length of the sprayed foil (nozzle sprays while moving back and forth). After spraying a layer, the films were dried (110 °C) for 20 seconds before the next layer was deposited on top. The used sample-to-nozzle distance was 20 cm and the used driving gas was nitrogen at a pressure of 1 bar. For pure TCNF foils, the first 20 single layers were sprayed at a low flow rate of 5.5 L min^{-1} in order to ensure a very homogenous TCNF coating with an ultra-low roughness. After that, 60 double layers were sprayed on top at a constant flow rate of 6.5 L min^{-1} to achieve the final thickness of 2 ± 1 µm. Top AgNW-TCNF foils were initially prepared just like pure TCNF foils, and then 10 double layers of AgNW-TCNF ink at a flow rate of 5.2 L min^{-1} were sprayed on top. For Embedded AgNW-TCNF foils the TCNF ink and the AgNW-TCNF ink were sprayed alternately, starting with 5 double layers of AgNW-TCNF ink at 5.5 L min^{-1}, followed by 10 double layers of TCNF ink at 6.5 L min^{-1}, then again 5 double layers of

AgNW-TCNF ink at 6.5 L min^{-1} and so on. In total, 25 double layers of AgNW-TCNF, and 40 double layers of TCNF were sprayed. For PEDOT:PSS-TCNF foils first 20 single layers and then twenty double layers of the PEDOT:PSS-TCNF ink were sprayed at a flow rate of 6.5 L min^{-1}.

After spraying the foils, the frames were removed from the silicon substrate. Subsequently, all samples except PEDOT:PSS-TCNF samples were put into a deionized water bath for 10 minutes at room temperature to delaminate the foils. The foils were taken out of the water using a nylon filter (40 µm) and pressed (4700 Pa) between two filter papers for 24 hours in order to prevent shrinking and winkles during the drying process. For PEDOT:PSS-TCNF foils, the same procedure was used, but the substrate was PDMS. No water bath was necessary for delamination of PEDOT:PSS-TCNF foils. Instead, the foils were simply peeled off using a tweezer and no pressing took place. An overview over the different samples were given in Figure S1 (Supporting Information).

Scanning Electron Microscopy: SEM measurements were conducted using a ZEISS Crossbeam 550L FE-SEM using the SESI detector. The acceleration voltage was 1–3 kV (depending on the material to be investigated) at a working distance of 2.8 – 4.7 mm. All samples were sputtered with a thin layer of Gold of 4 nm, obtained at 2.2 mA at a pressure of 100 mbar for 12 seconds. Pore sizes were estimated based on SEM images, which were analyzed using the software ImageJ.[51] Details can be found in the Supporting Information.

Atomic Force Microscopy and Roughness Measurements: Atomic force microscopy measurements were conducted using a Bruker Multi Mode 8 in Peak Force QNM mode with an Al coated silicon tip on nitride lever (T: 650 nm, L: 115 nm, f: 70 kHz, model scanasyst-air). The images were taken at an average scan rate of 0.88 Hz. The roughness was calculated based on the 5 × 5 $µm^2$ large AFM images. Analysis was done using the software Gwyddion (v2.56).

Conductivity and Resistance Measurements: Conductivity measurements were done using a four-point probe T2001A (Ossila Ltd., UK). The conductivity was measured before the delamination of the foils from the substrate. The target current was 2000 µA, the space between the four probes was 1.27 mm, and the maximum voltage was 10 V at a voltage increment of 0.01 V. Three different samples per foil type were measured and the average value was taken. The data was monitored and analyzed by the software Ossila Sheet Resistance (v2.0.3.1, Ossila Ltd, UK). Line resistance measurements were done using a FLUKE 73 III Multimeter after the delamination of the free-standing foils from the substrate.

UV–Vis Measurements: A custom-built setup consisting of a balanced deuterium tungsten source (DH-2000-BAL, Ocean Insight, 210–2500 nm), a spectrometer (OCEAN-FX-XR1_ES, Ocean Insight, 200–1025 nm), two collimation lenses (UV fused silica, CVA100-COL, LA4647, Thorlabs Inc., transparent wavelength range 185–2100 nm), and two optical fibers (QP600-1-SR-BX, Ocean Insight, 600 µm) was used for optical transmission measurements. The software package OceanView version 1.6.5 (Lite) (Ocean Insight) was used to analyze the data.

Tensile Testing: Tensile tests were performed using an Instron tensile tester (single column) with a 250 N load cell, a pressure of grips of 5 bar, and a stretching rate of 5% min^{-1}. The foils had a strip shaped geometry with an effective sample dimension (initial length x width) of 30 × 5 mm. The samples were attached to a paper frame using liquid glue. The frame was cut on both sides before the measurement. At least three samples of each foil type were tested. Young's modulus was determined by fitting the slope of the initial linear part of the measured stress-strain-curves using the software Origin 2022b.

Contact Angle Measurements: The water contact angle (WCA) on the surface was measured with a "Drop shape analyzer DSA25E" by Krüss in the "sessile drop"-configuration. The droplet volume was 20 µL. The droplet shape was fitted with an elliptical fit using the software shipped with the instrument.

Thickness Measurements: Foil thickness was measured using an ABSOLUTE Digimatic Indicator (Mitutoyo). Five foils of each type were measured. The results were averaged.

GIWAXS Measurements: Grazing incidence wide angle X-ray scattering (GIWAXS) measurements were performed at the beamline P03[52] at PETRA III, DESY at an energy of 11.87 keV, an incident angle of 0.12°, an SDD of 261 mm and a beam size of around 30 × 30 $µm^2$. The data were collected using a LAMBDA 9 M detector with a pixel size of 55 × 55 $µm^2$. The MATLAB toolbox GIXSGUI[53] was used for data analysis. For GIWAXS measurements, the foils were measured as deposited on the Si substrate and 15 single images per sample were taken, each at a new position in order to prevent beam damage.

FTIR Measurements: Fourier-transform infrared spectroscopy (FTIR) analysis was done using a Perkin Elmer Spectrum 100 FT-IR Spectrometer with a MIR TGS detector. The tested range was 600 to 4000 cm^{-1}. Sixteen scans per measurement were averaged, baseline corrected, and normalized to the carbonyl signal (1732 cm^{-1}) by the instrument's software Spectrum V10.5.1.

Statistical Analysis: Standard analysis was used as done in physics for calculating averages and standard deviations. Error propagation was done using standard statistical analysis. The data presentation was mean ± SD. Statistical analysis was done using the software Origin 2022b 64-Bit. GIWAXS image corrections were done automatically by the software GIXSGUI version 1.7.3. The UV–vis spectra were smoothed using the Adjacent Averaging method with 10 data points around each measurement point. During each conductivity measurement 25 single values were taken and their average value was calculated automatically by the software Ossila Sheet Resistance (v2.0.3.1, Ossila Ltd, UK).

Supporting Information

Supporting Information is available from the Wiley Online Library or from the author.

Acknowledgements

M. B. and S. V. R. thank DSF under grant DSF-33 "Investigation of processes for fabricating functional multicomponent stacks based on nanopaper and spray-coating" for funding. Y. L. and P. M-B. acknowledge the funding from the Deutsche Forschungsgemeinschaft (DFG, German Research Foundation) under Germany´s Excellence Strategy – EXC 2089/1 – 390776260 (e-conversion) and from TUM.solar in the context of the Bavarian Collaborative Research Project Solar Technologies Go Hybrid (SolTech). Y.L. acknowledge the financial support from the China Scholarship Council (CSC, grant no. 201906880006). The work has been

financially supported by the MML-POF IV program of the HGF. The acknowledge DESY (Hamburg, Germany), a member of the Helmholtz Association HGF, for the provision of experimental facilities. Parts of this research were carried out at P03, PETRA III. The thank Matthias Schwartzkopf for his support during the experiments at DESY. We acknowledge the support of CUI: Advanced Imaging of Matter of the German Research Foundation (DFG) EXC 2056, Project ID 390715994. We also acknowledge the support of the Helmholtz-Lund International Graduate School (HELIOS, HIRS-0018).

Open access funding enabled and organized by Projekt DEAL.

Conflict of Interest

The authors declare no conflict of interest.

Data Availability Statement

The data that support the findings of this study are available from the corresponding author upon reasonable request.

Keywords

3D materials, cellulose, organic electronics, spray deposition, thin films

Received: March 5, 2024
Revised: May 6, 2024
Published online: May 20, 2024

[1] M. Mizumura, T. Kubo, T. Moriki, *Adapt & Evolve 2015: East Asian Materials and Techniques in Western Conservation. Proceedings from the International Conference of the Icon Book & Paper Group* **2015**, 43.
[2] C. H. Stephens, P. M. Whitmore, *Cellulose* **2013**, *20*, 1099.
[3] T. Saito, S. Kimura, Y. Nishiyama, A. Isogai, *Biomacromolecules* **2007**, *8*, 2485.
[4] A. Isogai, T. Saito, H. Fukuzumi, *Nanoscale* **2011**, *3*, 71.
[5] Y. Qing, R. Sabo, Y. Wu, J. Y. Zhu, Z. Cai, *Cellulose* **2015**, *22*, 1091.
[6] N. Mittal, F. Ansari, V. Gowda Krishne, C. Brouzet, P. Chen, P. T. Larsson, S. V. Roth, F. Lundell, L. Wågberg, N. A. Kotov, L. D. Söderberg, *ACS Nano* **2018**, *12*, 6378.
[7] R. J. Moon, A. Martini, J. Nairn, J. Simonsen, J. Youngblood, *Chem. Soc. Rev.* **2011**, *40*, 3941.
[8] H. P. S. Abdul Khalil, A. H. Bhat, A. F. Ireana Yusra, *Carbohydr. Polym.* **2012**, *87*, 963.
[9] S. J. Eichhorn, A. Etale, J. Wang, L. A. Berglund, Y. Li, Y. Cai, C. Chen, E. D. Cranston, M. A. Johns, Z. Fang, G. Li, L. Hu, M. Khandelwal, K. Y. Lee, K. Oksman, S. Pinitsoontorn, F. Quero, A. Sebastian, M. M. Titirici, Z. Xu, S. Vignolini, B. Frka-Petesic, *J. Mater. Sci.* **2022**, *57*, 5697.
[10] Y. Cui, J. Lin, Y. Wu, X. Yang, *J. Polym. Sci.* **2024**, *62*, 280.
[11] Q. Chen, B. Sochor, A. Chumakov, M. Betker, N. M. Ulrich, M. E. Toimil-Molares, K. Gordeyeva, L. D. Söderberg, S. V. Roth, *Adv. Funct. Mater.* **2022**, 32, 2208074.
[12] Y. Shchipunov, I. Postnova, *Adv. Funct. Mater.* **2018**, *28*, 1.
[13] H. Françon, Z. Wang, A. Marais, K. Mystek, A. Piper, H. Granberg, A. Malti, P. Gatenholm, P. A. Larsson, L. Wågberg, *Adv. Funct. Mater.* **2020**, 30, 1909383.
[14] W. Cao, C. Ma, D. Mao, J. Zhang, M. Ma, F. Chen, *Adv. Funct. Mater.* **2019**, *29*, 1905898.
[15] L. Hu, G. Zheng, J. Yao, N. Liu, B. Weil, M. Eskilsson, E. Karabulut, Z. Ruan, S. Fan, J. T. Bloking, M. D. McGehee, L. Wågberg, Y. Cui, *Energy Environ. Sci.* **2013**, *6*, 513.
[16] F. Catania, H. De Souza Oliveira, P. Lugoda, G. Cantarella, N. Münzenrieder, *J. Phys. D. Appl. Phys.* **2022**, *55*, 323002.
[17] Y. H. Kim, E. Lee, J. G. Um, M. Mativenga, J. Jang, *Sci. Rep.* **2016**, *6*, 1.
[18] H. K. Yogeenth Kumaresan, R. Lee, N. Lim, Y. Pak, G.-Y. J. W Kim, *Adv. Elect. Mater.* **2018**, *4*, 1800167.
[19] S.-W. Hwang, J.-K. Song, X. Huang, H. Cheng, S.-K. Kang, B. H. Kim, J.-H. Kim, S. Yu, Y. Huang, *Adv. Mater.* **2014**, *26*, 3905.
[20] F. Garnier, R. Hajlaoui, A. Yassar, P. Srivastava, *Science* **1994**, *265*, 1684.
[21] S. J. Royer, F. Greco, M. Kogler, D. D. Deheyn, *PLoS One* **2023**, *18*, e0284681.
[22] H. Fukuzumi, T. Saito, T. Iwata, Y. Kumamoto, A. Isogai, *Biomacromolecules* **2009**, *10*, 162.
[23] T. Lei, M. Guan, J. Liu, H. C. Lin, R. Pfattner, L. Shaw, A. F. McGuire, T. C. Huang, L. Shao, K. T. Cheng, J. B. H. Tok, Z. Bao, *Proc. Natl. Acad. Sci. USA* **2017**, *114*, 5107.
[24] H. Nadeem, M. Athar, M. Dehghani, G. Garnier, W. Batchelor, *Sci. Total Environ.* **2022**, *836*, 155654.
[25] K. Shanmugam, H. Doosthosseini, S. Varanasi, G. Garnier, W. Batchelor, *Cellulose* **2018**, *25*, 1725.
[26] D. Beneventi, E. Zeno, D. Chaussy, *Ind. Crops Prod.* **2015**, *72*, 200.
[27] K. Shanmugam, S. Varanasi, G. Garnier, W. Batchelor, *Cellulose* **2017**, *24*, 2669.
[28] C. Lin, Q. Wang, Q. Deng, H. Huang, F. Huang, L. Huang, Y. Ni, L. Chen, S. Cao, X. Ma, *Cellulose* **2019**, *26*, 4061.
[29] W. Yang, L. Jiao, W. Liu, H. Dai, *Nanomaterials* **2019**, 9.
[30] G. Hou, G. Li, H. Chen, Z. Fang, *Chem. Eng. J.* **2022**, *439*, 135776.
[31] M. Betker, C. Harder, E. Erbes, J. E. Heger, A. E. Alexakis, B. Sochor, Q. Chen, M. Schwartzkopf, K. Volker, P. Mu, K. Schneider, S. A. Techert, L. S. Daniel, S. V Roth, *ACS. Appl. Nano Mater* **2023**, *6*, 13677.
[32] J. T. Del Mundo, S. Rongpipi, H. Yang, D. Ye, S. N. Kiemle, S. L. Moffitt, C. L. Troxel, M. F. Toney, C. Zhu, J. D. Kubicki, D. J. Cosgrove, E. W. Gomez, E. D. Gomez, *Sci. Rep.* **2023**, *13*, 5421.
[33] D. Beneventi, D. Chaussy, D. Curtil, L. Zolin, C. Gerbaldi, N. Penazzi, *Ind. Eng. Chem. Res.* **2014**, *53*, 10982.
[34] H. Nadeem, M. Naseri, K. Shanmugam, C. Browne, G. Garnier, W. Batchelor, *Cellulose* **2020**, *27*, 10225.
[35] J. Wang, X. Zhu, P. Xiong, J. Tu, Z. Yang, F. Yao, M. Gama, Q. Zhang, H. Luo, Y. Wan, *J. Mater. Chem. A* **2022**, *10*, 960.
[36] Y. Chen, L. Pang, Y. Li, H. Luo, G. Duan, C. Mei, W. Xu, W. Zhou, K. Liu, S. Jiang, *Compos. Part A Appl. Sci. Manuf.* **2020**, 135.
[37] H. Koga, T. Saito, T. Kitaoka, M. Nogi, K. Suganuma, A. Isogai, *Biomacromolecules* **2013**, *14*, 1160.
[38] C. Wan, Y. Jiao, J. Li, *J. Mater. Chem. A* **2017**, *5*, 17267.
[39] M. Wakabayashi, S. Fujisawa, T. Saito, A. Isogai, *Front. Chem.* **2020**, *8*, 37.
[40] H. Du, M. Zhang, K. Liu, M. Parit, Z. Jiang, X. Zhang, B. Li, C. Si, *Chem. Eng. J.* **2022**, *428*, 131994.
[41] A. Khakalo, T. Mäkelä, L. S. Johansson, H. Orelma, T. Tammelin, *ACS Appl. Bio Mater.* **2020**, *3*, 7428.
[42] C. J. Brett, O. K. Forslund, E. Nocerino, L. P. Kreuzer, T. Widmann, L. Porcar, N. L. Yamada, N. Matsubara, M. Månsson, P. Müller-Buschbaum, L. D. Söderberg, S. V. Roth, *Adv. Electron. Mater.* **2021**, *7*, 2100137.
[43] G. F. Wang, X. M. Tao, J. H. Xin, B. Fei, *Nanoscale Res. Lett.* **2009**, *4*, 613.
[44] J. Dong, G. Portale, *Adv. Mater. Interfaces* **2020**, 7.
[45] G. S. Lee, H. J. Kwon, T. K. An, Y. H. Kim, *Chem. Commun.* **2023**, *59*, 4995.
[46] A. M. Rahmatika, Y. Toyoda, T. T. Nguyen, K. L. A. Cao, T. Hirano, T. Kitamura, Y. Goi, Y. Morita, T. Ogi, A. C. S. Appl, *Polym. Mater.* **2022**, *4*, 6700.

[47] M. Österberg, K. A. Henn, M. Farooq, J. J. Valle-Delgado, *Chem. Rev.* **2023**, *123*, 2200.
[48] K. Lichtenstein, N. Lavoine, *Polym. Degrad. Stab.* **2017**, *146*, 53.
[49] L. Salmén, J. S. Stevanic, *Cellulose* **2018**, *25*, 6333.
[50] J. Dong, J. Liu, X. Qiu, R. Chiechi, L. J. A. Koster, G. Portale, *Engineering* **2021**, *7*, 647.
[51] M. D. Abràmoff, P. J. Magalhães, S. J. Ram, *Biophotonics Int.* **2004**, *11*, 36.
[52] A. Buffet, A. Rothkirch, R. Döhrmann, V. Körstgens, M. M. Abul Kashem, J. Perlich, G. Herzog, M. Schwartzkopf, R. Gehrke, P. Müller-Buschbaum, S. V. Roth, *J. Synchrotron Radiat.* **2012**, *19*, 647.
[53] Z. Jiang, *J. Appl. Crystallogr.* **2015**, *48*, 917.